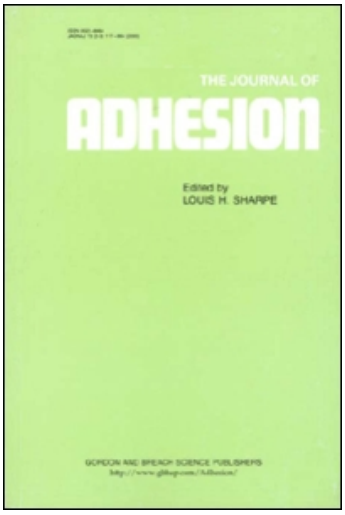

The Journal of Adhesion
Publication details, including instructions for authors and subscription information:
http://www.informaworld.com/smpp/title~content=t713453635

Peeling of Elastic Tapes: Effects of Large Deformations, Pre-Straining, and of a Peel-Zone Model

Alain Molinari[a]; Guruswami Ravichandran[b]
[a] Laboratoire de Physique et Mécanique des Matériaux, Université Paul Verlaine-Metz, Ile du Saulcy, Metz, France [b] Graduate Aeronautical Laboratories, California Institute of Technology, Pasadena, California, USA

To cite this Article Molinari, Alain and Ravichandran, Guruswami(2008) 'Peeling of Elastic Tapes: Effects of Large Deformations, Pre-Straining, and of a Peel-Zone Model', The Journal of Adhesion, 84: 12, 961 — 995
To link to this Article: DOI: 10.1080/00218460802576995
URL: http://dx.doi.org/10.1080/00218460802576995

The Journal of Adhesion, 84:961–995, 2008

ISSN: 0021-8464 print/1545-5823 online
DOI: 10.1080/00218460802576995

Taylor & Francis
Taylor & Francis Group

Peeling of Elastic Tapes: Effects of Large Deformations, Pre-Straining, and of a Peel-Zone Model

Alain Molinari[1] and Guruswami Ravichandran[2]
[1]Laboratoire de Physique et Mécanique des Matériaux, Université Paul Verlaine-Metz, Ile du Saulcy, Metz, France
[2]Graduate Aeronautical Laboratories, California Institute of Technology, Pasadena, California, USA

A peel model for non-linear elastic tapes is presented which accounts for large deformations and for pre-straining. The large deformation setting is a new feature of modelling, which would be of interest for applications related to soft polymers and tissues. The conditions for having quasistatic-steady debonding or dynamic catastrophic debonding are determined in terms of the loading variables (peel angle and peeling force). The decohesion energy associated with a given process-zone model is included in the formulation of the peeling model. The predictions of various decohesion laws are discussed with respect to experimental results in the literature. Finally, the adhesion of a gecko is analysed and the maximum adhesion force of a single spatula is evaluated. The result correlates well with the maximum experimental pulling force reported in the literature for a gecko's seta.

Keywords: Gecko adhesion; Large deformation; Non-linear elasticity; Peel test; Peel-zone model; Pre-strain

1. INTRODUCTION

Peeling of adhesive joints is important in many technological applications. This problem is also of great interest in biological sciences, like the remarkable ability of some animals to climb walls and walk on ceilings. The modelling of peeling has gained considerable interest in recent years in relationship to the analysis of biological adhesive systems. For instance, the adhesive system of the gecko's toes provide remarkable climbing abilities [1–3]. The toes contain setal arrays with

Received 2 June 2008; in final form 22 September 2008.
Address correspondence to Alain Molinari, Laboratoire de Physique et Mécanique des Matériaux, Université Paul Verlaine-Metz, Ile du Saulcy, F-57045 Metz Cedex 01, France. E-mail: molinari@lpmm.univ-metz.fr

hundreds of spatulae on each seta. The intimate contact between the toes and surfaces is due to this hierarchical structure and the multiplicity of very fine spatulae. This is an example of optimal design of nature, which has attracted a lot of attention and is an inspiration for designing new dry adhesives.

Recently, Pesika *et al.* [4] have considered the peeling of pressure-sensitive adhesive tapes from a rigid substrate and have pointed to some analogy with the gecko's adhesion problem. While Tian *et al.* [5] have characterized the pulling force generated by the adhesion and friction of a single gecko spatula, by considering van der Waals forces between the adhering surfaces, Pesika *et al.* [4] have developed a macroscopic analysis to model the spatula adhesion. This peel-zone model (henceforth denoted as PPZ model) [4] is based on the microscopic observation of the geometry of the peel zone during the tape detachment. The model does not account for the tape extensibility and is not able to correlate with the experimental data at small peel angles for tapes with low stretch modulus.

The aim of this paper is to propose a general peeling model accounting for the tape extensibility and to provide a framework encompassing any peel-zone model. For a rigid substrate, the peel force is a function of decohesion energy, the mechanical properties of the tape-backing and the peel angle. For given mechanical properties of the tape-backing, decohesion energy can be characterized from measurements of the peel force at various peel angles. Defining the law governing the decohesion energy is a difficult problem as this energy may depend on the peel angle, peel rate, temperature, relative humidity, and dwell time after attachment. In this paper, the velocity dependence of the debonding energy shall not be considered. The peeling tests are assumed to be performed under prescribed peeling rates. Contrary to peel models which assume tape inextensibility, the load-extension response of the tape is an important input in the present modelling. For the sake of generality, a large deformation framework is adopted here. This new feature of the modelling together with the ability to account for non-linear elastic response can be of importance in applications related to soft polymers and tissues in bioengineering. For tapes with low stretch modulus, the elongation can be substantial at small peel angles. In this case, large deformations have to be accounted for in order to predict the peel force correctly. This point is illustrated by comparing the results of the present approach with the peeling model of Williams and Kauzlarich [6], which accurately characterizes the peel force when the deformation of the tape remains small but becomes less accurate at large deformations.

In general, the tape can undergo pre-straining during the bonding operation with the substrate. The effect of pre-strain on the peeling force is analysed in detail in this paper. By assuming that the debonding energy is rate independent, the conditions for having quasistatic and steady, or dynamic (catastrophic) debonding are determined under force control (given peel angle and peeling force).

The paper is organized as follows. In Section 2, a large deformation setting is developed to model the peel test of non-linear elastic adhesive tapes, which accounts for the tape pre-straining. The conditions for (i) stable adhesion, (ii) quasistatic-steady decohesion, and (iii) dynamic decohesion are analysed for a prescribed pulling force which is assumed to be time independent. In Section 3, the model is compared with experimental results from the literature. A parametric analysis is then performed to elucidate the effects of large deformations and pre-straining. In Section 4, the peel-zone model of Pesika *et al.* [4] is extended to account for the tape's elastic response and the results are then compared with experimental data. Finally, an application of the model to the gecko's adhesion system is considered. The maximum adhesion force exerted on a single spatula is evaluated and is found to be well correlated with experimental measurements of the maximum load bearing capacity of the gecko's seta reported in the literature.

2. PEELING MODEL ACCOUNTING FOR NON-LINEAR ELASTICITY AND LARGE DEFORMATIONS

A schematic illustration of the steady-state peeling process of a tape is shown in Fig. 1. The peel angle has a given value θ and a constant

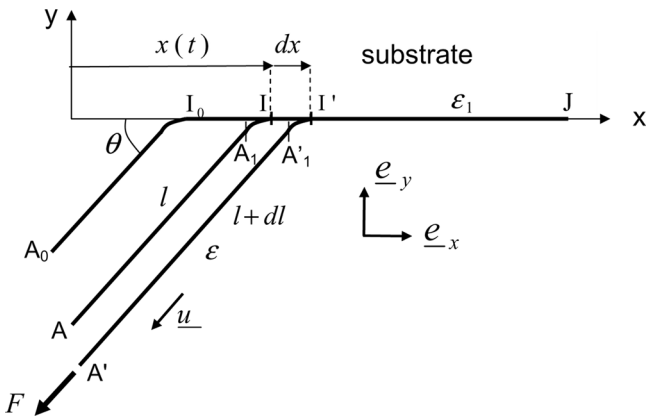

FIGURE 1 Schematic of the tape peel test.

peeling force F is applied. The tape is assumed to be infinitely flexible (negligible bending [flexion] stiffness). The cross-section of the tape is rectangular (width, b, and thickness, h). The substrate is considered to be rigid (no deformation) and the tape is assumed to behave elastically. The theory is presented in a large deformation setting.

2.1. Calculation of the Peeling Force in Terms of the Peel Angle

Our aim is to determine the peeling force, F, in terms of the peel angle, θ, and of the mechanical characteristics of the tape and the adhesive layer. The peeling process is assumed to be stationary; therefore, the peeling force does not depend on time. Detachment occurs along a process zone limited by points, A_1 and I, see Fig. 1. For a steady process, the shape of the process zone remains invariant with time. Debonding is initiated at I and is completed at the exit of the process zone A_1. We denote by $x(t)$ the position of the tip I of the process zone at time t.

The true strain, ε, is uniform along the portion AA_1 of the tape which is completely detached from the substrate. The strain, ε, is defined by $\varepsilon = \ln(l/L_0)$, where L_0 is the initial length of the tape element (before bonding to the substrate) and l is the current length. The tape is assumed to have an elastic response, possibly non-linear. The dependence of the tensile force, $F(\varepsilon)$, in terms of the strain, ε, is identified from a simple tension test. The strain, ε, is assumed to be smaller than the critical value for which necking occurs. Plastic yielding and strain rate dependence are disregarded. Peeling tests are assumed to be conducted at constant temperature, relative humidity, and dwell time.

At time t, the tape is bonded to the substrate along IJ, see Fig. 1. The detachment process is initiated at I and evolves along the process zone until complete debonding is achieved at A_1. We denote by dx the progress of the process zone from I to I' realized during the time increment, dt. The new length of the completely detached tape is $A'A'_1 = l + dl$.

Denoting by dW_{ext} the elementary work of the peel force, F, associated with the progress of the process zone by a distance dx, the following relationship is obtained from energy balance:

$$dW_{ext} = dW_{el} + dW_{peel}, \tag{1}$$

where dW_{el} is the increment of the elastic energy of the tape (the substrate is assumed to be infinitely rigid). The decohesion energy to produce complete debonding along the distance dx has the form:

$$dW_{peel} = \gamma_1 b_1 dx, \tag{2}$$

where b_1 is the width of attached tape and γ_1 is the energy per unit area (of attached tape) required to have complete detachment. The tape has an initial pre-strain, ε_1, due to the pre-tensioning during bonding to the substrate. The tape element with initial length dL_0 is stretched during the bonding process to the length dL. The resulting pre-strain is $\varepsilon_1 = \ln(dL/dL_0)$. The initial width, b, of the stress free tape is changed into b_1 after attachment.

The elastic energy stored in the tape element which has the length dL after bonding is denoted by dW_{el}^{BD}. This elastic energy, available before debonding (superscript BD), is evaluated in Appendix A:

$$dW_{el}^{BD} = dL \int_0^{\varepsilon_1} F(\varepsilon') \exp(\varepsilon' - \varepsilon_1) d\varepsilon'. \tag{3}$$

When debonding has progressed along the distance dx, the new state of the system can be described by considering that the element with length $dL = dx$ and prestrain $\varepsilon_1 = \ln(dL/dL_0)$ before debonding (*i.e.,* just before entering into the process zone) is transformed into the tape element just after exiting the process zone with strain $\varepsilon = \ln(dl/dL_0)$. After complete detachment (superscript AD), the tape element with strain ε has the elastic energy, see Appendix A:

$$dW_{el}^{AD} = dL \int_0^{\varepsilon} F(\varepsilon') \exp(\varepsilon' - \varepsilon_1) d\varepsilon'. \tag{4}$$

Thus, for a progress of debonding by the increment $dL = dx$, the variation of the elastic energy of the system is:

$$dW_{el} = dW_{el}^{BD} - dW_{el}^{AD} = dx \int_{\varepsilon_1}^{\varepsilon} F(\varepsilon') \exp(\varepsilon' - \varepsilon_1) d\varepsilon'. \tag{5}$$

The peel force $\underline{F} = F(\varepsilon)\underline{u}$ is collinear with the unit vector, $\underline{u} = -\cos\theta \underline{e}_x - \sin\theta \underline{e}_y$, where $\underline{e}_x$ and $\underline{e}_y$ are unit vectors defined in Fig. 1. The incremental work of the peeling force is given by $dW_{ext} = \underline{F} \cdot \underline{AA'}$ with $\underline{AA'} = dl\underline{u} + dx\underline{e}_x$. Thus, considering that $dl = \exp(\varepsilon) dL_0 = \exp(\varepsilon - \varepsilon_1) dx$, we have:

$$dW_{ext} = -F(\varepsilon)\cos(\theta) dx + F(\varepsilon) dl = -F(\varepsilon)\cos(\theta) dx + F(\varepsilon)\exp(\varepsilon - \varepsilon_1) dx.$$

By combining this relationship with Eqs. (1), (2), and (5), it follows that:

$$F(\varepsilon)\exp(\varepsilon - \varepsilon_1) - F(\varepsilon)\cos(\theta) - \int_{\varepsilon_1}^{\varepsilon} F(\varepsilon')\exp(\varepsilon' - \varepsilon_1) d\varepsilon' - \gamma_1 b_1 = 0. \tag{6}$$

The bonding energy, γ_1, per unit area, of the attached tape is in general a function of the pre-strain, ε_1, and of the bonding energy, γ, per unit area, of the unstretched tape. Characterizing this functional dependence is still an open subject; for illustrative purposes, a specific case is discussed in Appendix B. However, for applications considered in this paper, the prestrain is in general small. As a first approximation, the changes in the geometry of the tape can be disregarded. Thus, one assumes that $b = b_1$ and $\gamma = \gamma_1$. Under this assumption, Eq. (6) takes on the form:

$$F(\varepsilon)\exp(\varepsilon - \varepsilon_1) - F(\varepsilon)\cos(\theta) - \int_{\varepsilon_1}^{\varepsilon} F(\varepsilon')\exp(\varepsilon' - \varepsilon_1)d\varepsilon' - \gamma b = 0. \quad (7)$$

For a given peel angle, θ, pre-strain, ε_1, and tape force-deformation response, $F(\varepsilon)$, the relationship in Eq. (7) allows one to determine the strain, ε, of the tape after complete detachment and finally to get the peeling force, F, itself from the constitutive relationship, *i.e.*, $F(\varepsilon)$ in terms of ε.

When γ is independent of θ, Eq. (7) gives $\cos\theta$ as a function of ε. Thus, the function $\theta(\varepsilon)$ is known and the graph $F - \theta$ is easily obtained by the parametric representation, namely, $(\theta(\varepsilon), F(\varepsilon))$.

For inextensible tapes, Eq. (7) simplifies and the peeling force has the form

$$F = \frac{\gamma b}{1 - \cos\theta}. \quad (8)$$

The above equation due to Rivlin [7] is widely known in modelling peeling of inextensible tapes.

In the case of relatively small deformations, using Eq. (7), the peeling force can be expressed by a second order expansion in terms of deformation: $F(\varepsilon) = S_0(E\varepsilon + E_2\varepsilon^2)$ with S_0 being the initial cross-sectional area of the stress-free tape. Then, by expanding the relationship in Eq. (7) to the second order with respect to ε and ε_1, we have:

$$\frac{1}{2}S_0E\left((\varepsilon - \varepsilon_1)^2 + 2\varepsilon^2\frac{E_2}{E}(1 - \cos\theta)\right) + S_0E\varepsilon(1 - \cos\theta) - \gamma b = 0. \quad (9)$$

It can be easily checked that, to the order two in ε and ε_1, Eq. (9) is identical to:

$$\frac{1}{2ES_0}(F - F_1)^2 + F(1 - \cos\theta) - \gamma b = 0, \quad (10)$$

where $F_1 = F(\varepsilon_1)$ is the pre-tension force in the tape before debonding. The expression in Eq. (10) generalizes the well known Kendall's

formula [8], by accounting for the pre-straining, ε_1, of the tape and by considering a nonlinear dependence of the peeling force with respect to the deformation ε. The influence of the tape pre-strain was analysed in [9].

The framework adopted here generalizes the approaches of Williams and Kauzlarich [6,9]. The present formulation accounts for large deformations by using true strain rather than engineering strain, which may be important in some applications. Making use of engineering strain, the result of Williams and Kauzlarich [6].

$$(1-\varepsilon_1)(1+\varepsilon)F(\varepsilon) - F(\varepsilon)\cos\theta - \int_{\varepsilon_1}^{\varepsilon} F(\varepsilon')d\varepsilon' - \gamma b = 0, \qquad (11)$$

agrees with Eq. (7) for relatively small deformations, but differs for large deformations. This point will be illustrated later.

2.2. Quasistatic and Dynamic Peeling Processes

The peeling force obtained from the energy balance Eq. (1) has been obtained for a quasistatic stationary process. The state of the system is defined by the amplitude of the applied force, F, the value of the peel angle, θ, the pre-strain, ε_1, and the position, x, of the tip of the process zone. For a given state and given boundary conditions, it is worthwhile to analyse the conditions under which the debonding process occurs under quasistatic or under dynamic conditions. As in Section 2.1, the applied force, $\underline{F}$, is constant, or equivalently F and θ are constant.

The potential energy of the system is:

$$W_{pot} = W_{el} + W_F, \qquad (12)$$

where W_{el} is the total elastic energy and $W_F = -\underline{F} \cdot \underline{OA}$ is the potential energy of the applied force $\underline{F}$.

For a given displacement, dx, of the process zone tip, the energy, $-dW_{pot}$, is extracted from the system. This energy has to be compared with the debonding energy, $dW_{peel} = \gamma b dx$. When $-dW_{pot} < \gamma b dx$, the system does not provide enough energy for debonding to occur, thus, the rate of peeling is $\dot{x} = 0$. If $-dW_{pot} = \gamma b dx$, quasistatic debonding occurs, $\dot{x} > 0$. The energy balance Eq. (1) is retrieved (with $dW_{ext} = -dW_F$) and peeling is governed by Eq. (7). If $-dW_{pot} > \gamma b dx$, the energy released from the system is in excess with respect to the energy consumed by debonding. When rate effects are neglected, the excess of energy is transformed into kinetic energy and the debonding process is dynamic and catastrophic for the force controlled conditions and the constant debonding energy considered here.

The energy release rate per unit tape-width is defined in the usual manner:

$$G = -\frac{1}{b}\frac{dW_{pot}}{dx}. \tag{13}$$

Using Eq. (12) together with the relationship $dW_{ext} = -dW_F$ and the results of Eqs. (5) and (6), we obtain:

$$G(\varepsilon, \varepsilon_1, \theta) = \frac{F(\varepsilon)}{b}[\exp(\varepsilon - \varepsilon_1) - \cos\theta] - \int_{\varepsilon_1}^{\varepsilon} \frac{F(\varepsilon')}{b}\exp(\varepsilon' - \varepsilon_1)d\varepsilon'. \tag{14}$$

With the notation:

$$G_c = \gamma, \tag{15}$$

the discussion can be summarized as:

$$\dot{x} = 0 \quad \text{for} \quad G < G_c \quad \text{(no debonding)}, \tag{16a}$$

$$\dot{x} > 0 \quad \text{for} \quad G = G_c \quad \text{(quasistatic debonding)}, \tag{16b}$$

$$\dot{x} > 0 \quad \text{for} \quad G > G_c \quad \text{(dynamic debonding)}. \tag{16c}$$

The condition in Eq. (16b) is precisely the one obtained in Eq. (7). When this condition is met, it is worth noting that G remains constant. This is due to Eq. (14) and the time independence of θ (loading condition) and of ε [consequence of Eq. (7)]. Therefore, the critical condition in Eq. (16b) remains satisfied at all times and the debonding process is stationary.

3. RESULTS AND DISCUSSION

The effects of the elastic stiffness and of large deformations are first analysed by considering a 3M-Magic® tape (3M, St. Paul, MN, USA) with a cellulose backing and a synthetic acrylic adhesive adherent to a PTFE substrate as studied in [6]. The tape width and thickness are $b = 19\,\text{mm}$ and $h = 0.05\,\text{mm}$, respectively. The mechanical response of the tape is linearly elastic with Young's modulus $E = 1.67\,\text{GPa}$ up to the yield strain of 0.018:

$$F = ES_0\varepsilon, \tag{17}$$

where S_0 is the initial cross section of the tape in the stress-free state.

The debonding energy per unit surface is $\gamma = 10\,\text{J/m}^2$ and is shown in [6] to be independent of the peel angle. Figure 2(a) shows the peeling

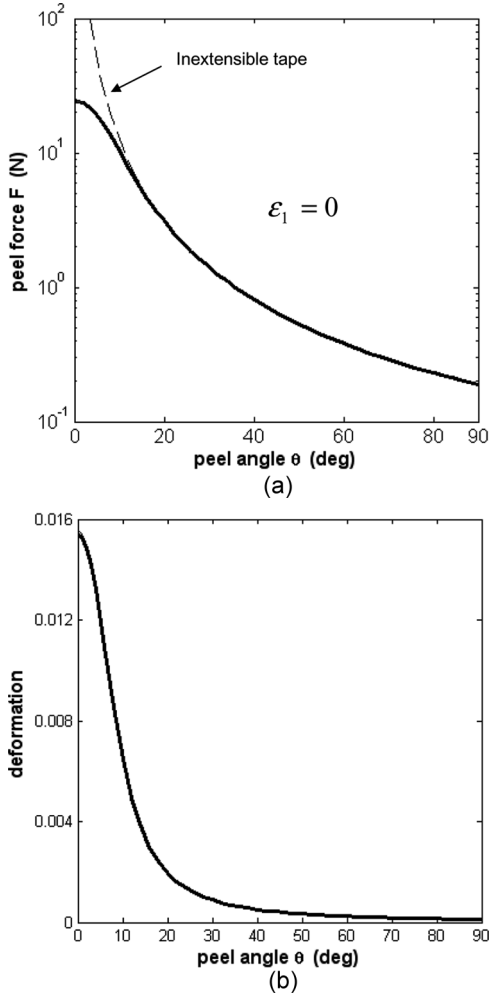

FIGURE 2 (a) Peeling force in terms of the peel angle for a 3M-Magic tape on a PTFE substrate studied by Williams and Kauzlarich [6]. The response of the tape is linear elastic with Young's modulus, $E = 1.67\,\text{GPa}$. The debonding energy $\gamma = 10\,\text{J/m}^2$ is assumed to be independent of the peel angle. The pre-strain is $\varepsilon_1 = 0$. The models in Eqs. (7), (9), and (11) give the same results. (b) Deformation in terms of peel angle.

force, F, in terms of the peel angle for $0 \leq \theta \leq 90^\circ$ in a semi-logarithmic plot. For reference, we have also plotted in Fig. 2(a) the peeling force for an inextensible tape given by Eq. (8).

For this material with relatively high stretching modulus, the deformation remains small as shown in Fig. 2(b). Therefore, the predictions of the large deformation theory given by Eq. (7) and of the small deformation approach given by Eq. (11) are almost identical (but situations where these models provide different results will be seen later). These results are in good correlation with the experimental data as shown by Williams and Kauzlarich [6]; see their Fig. 5 where Eq. (11) was used to compare with experiments. Note that in Fig. 2(b) the deformations predicted by Eq. (7) and (10) are identical and that the maximum strain obtained for $\theta = 0$ is smaller than the yield strain, 0.018. Thus, the response of the tape remains linearly elastic. In that case, the Kendall formulation Eq. (9) (with no pre-straining, *i.e.*, $F_1 = 0$) also provides correct results.

In Fig. 2, the pre-strain, ε_1, was assumed to be zero. In the experiments conducted on 3M-Magic tapes and PTFE substrate by Williams and Kauzlarich [6], the pre-deformation was less than 0.01 according to these authors. The effect of pre-strain is analysed in Fig. 3 for $\varepsilon_1 = 0$ (as in Fig. 2), $\varepsilon_1 = 0.005$, and $\varepsilon_1 = 0.01$. Here, again, the results predicted by Eqs. (7), (9), and (11) are in close agreement, the maximum difference being around 2.5% at $\theta = 0$ for $\varepsilon_1 = 0.01$. Only the results corresponding to (7) are presented. It is shown in Fig. 3 that at small values of the peel angle, the peeling force and the strain, ε, are increasing with ε_1.

This feature can be easily demonstrated for $\theta = 0$. The strain in the tape after complete detachment is denoted by $\hat{\varepsilon}(\varepsilon_1)$ since it is function of the pre-strain, ε_1. Consider two different pre-strains, ε_1 and ε_1^*, and denote by F and F^* the corresponding peeling forces, by F_1 and F_1^* the pretension forces, and by $\hat{\varepsilon}(\varepsilon_1)$ and $\hat{\varepsilon}(\varepsilon_1^*)$ the strains in the detached tape (also denoted by $\hat{\varepsilon}$ and $\hat{\varepsilon}^*$). Due to the linear elastic response and small deformations, the generalized Kendall's formula in Eq. (10) can be used as it gives the same results as the general approach in Eq. (7). From Eq. (10), we have at $\theta = 0$, $F = F_1 + \sqrt{2ES_0\gamma b}$, and $F^* = F_1^* + \sqrt{2ES_0\gamma b}$, and by the difference:

$$F - F^* = F_1 - F_1^*. \tag{18}$$

The forces are related to strains by linear elasticity, thus, from Eq. (12) one has:

$$\hat{\varepsilon}(\varepsilon_1) - \hat{\varepsilon}(\varepsilon_1^*) = \varepsilon_1 - \varepsilon_1^*. \tag{19}$$

For $\varepsilon_1^* = 0$, it follows that $\hat{\varepsilon}(\varepsilon_1) = \hat{\varepsilon}(0) + \varepsilon_1$. Thus, it has been shown that, for $\theta = 0$, the deformation, $\hat{\varepsilon}(\varepsilon_1)$, in the tape after detachment is the superposition of the pre-strain, ε_1, and the deformation without

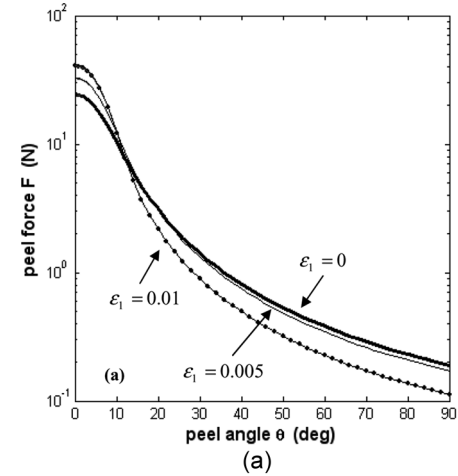

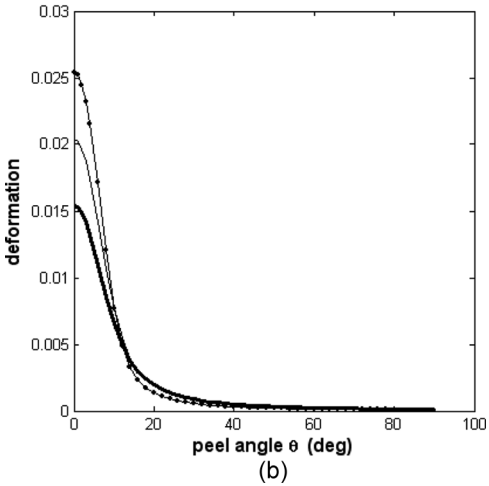

FIGURE 3 Effect of the pre-strain ε_1 on (a) the peeling force, (b) the strain after complete detachment. The results of the large deformation model Eq. (7) are almost identical with the small deformation model Eq. (11) and the modified Kendall model Eq. (9). The maximum difference between these models is 2.5% at $\theta = 0$ for $\varepsilon_1 = 0.01$. For clarity, only the results of the model Eq. (7) are shown.

pre-strain, $\hat{\varepsilon}(0)$. The results shown in Fig. 3(b) are clearly in agreement with this relationship.

When the pre-strain is increased ($\varepsilon_1 > \varepsilon_1^*$), it can be deduced from Eq. (18) and the linear force-deformation relationship that the peeling

force is also increased ($F > F^*$). This result obtained for $\theta = 0$ is also valid for small values of the peel angle as shown in Fig. 3(a).

For larger values of θ, it appears in Fig. 3(a) that the peeling force is a decreasing function of the pre-strain, contrary to the situation found for small values of θ. This is related to the release of the elastic energy stored during the bonding process. During debonding, the deformation in the tape decreases and part of the stored energy is released and contributes to the detachment process, thereby reducing the level of the external work and of the peeling force necessary for debonding.

We consider now a tape whose force-extension relationship is described by a power-law:

$$F = B\varepsilon^n. \tag{20}$$

In Fig. 4(a) the corresponding dependence of the peeling force is shown in terms of the peel angle for the decohesion energy $\gamma = 20\,\mathrm{J/m^2}$. The parameters in Eq. (20) are those for the 3M 33PVC electrical tape considered in [6]: $n = 0.51$; $B = 23.6\,\mathrm{N}$. The force extension diagram is represented in Fig. 4(c). Necking does not occur since according to Eq. (20) the force is increasing with deformation. In Fig. 4(a), the whole range of peel angle $0 \leq \theta \leq 180^\circ$ is considered to illustrate the perfect match of Eq. (7), for large enough θ, with the result Eq. (8) for inextensible tape. Note, however, that for this highly extensible tape it is shown in [6] that the peel force at $\theta = 180^\circ$ for no prestrain is near that which is measured at 90°, whereas the theory for inextensible tapes shows that peel force at 180° is equal to half that at 90°.

The information given in [6] by Williams and Kauzlarich on the adhesion energy was not sufficient to make a direct comparison with their experimental data. However, a parametric analysis can be carried out to evaluate the effect of the large deformation theory. For small peel angles, Figs. 4(a) and 4(b) indicate only a small deviation between the results given by the large deformation approach in Eq. (7) and those of the small deformation approach in Eq. (11). The results shown in Fig. 5 are obtained for a softer tape response with $B = 1.18\,\mathrm{N}$. The difference between the results of Eq. (7) and (11) is about 10% at small peel angles.

The effect of the pre-strain is analysed in Fig. 6. The conditions are the same as in Fig. 4 except for the value of pre-strain which was zero in Fig. 4 and is assumed here to be $\varepsilon_1 = 0.05$. A significant divergence between the predictions of Eqs. (7) (bold line) and (11) (line with markers) can be observed at small peel angles. As observed and commented on earlier in discussing Fig. 3, the comparison of Fig. 4(a) and

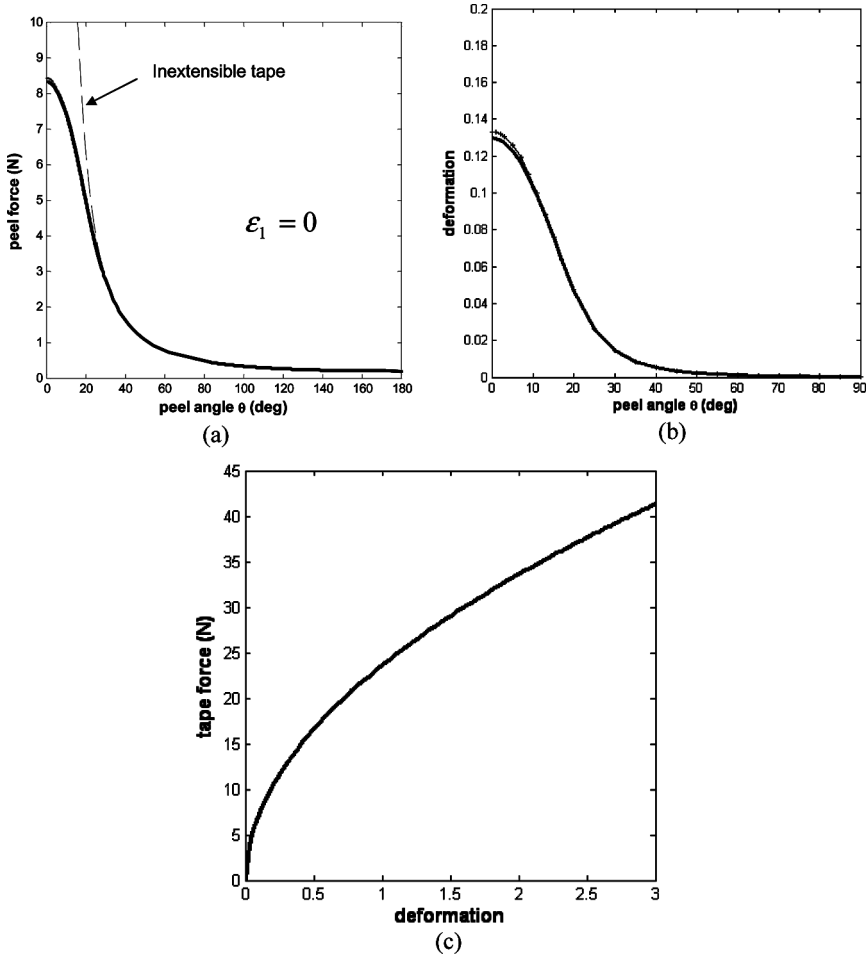

FIGURE 4 The peeling force and the tape deformation shown in (a) and (b) in terms of the peel angle θ are obtained for the force-extension power-law Eq. (15) represented in (c). The coefficients of the power-law ($n = 0.51$; $B = 23.6\,\mathrm{N}$) have been calibrated by Williams and Kauzlarich [6] so as to be representative of the response of the 3M 33 PVC electrical tape. The decohesion energy is $\gamma = 20\,\mathrm{J/m^2}$ and the pre-strain is zero. Note that the results in (a) and (b) given by Eq. (7) (bold solid line) are close to those of Eq. (11) (thin solid line with markers). In (a), the whole range of peel angle $0 \leq \theta \leq 180^\circ$ is considered to illustrate the perfect match, for large enough θ, with the result Eq. (8) for inextensible tape.

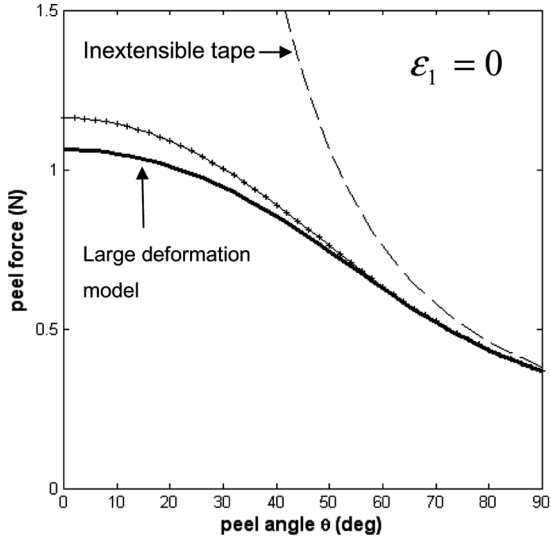

(a)

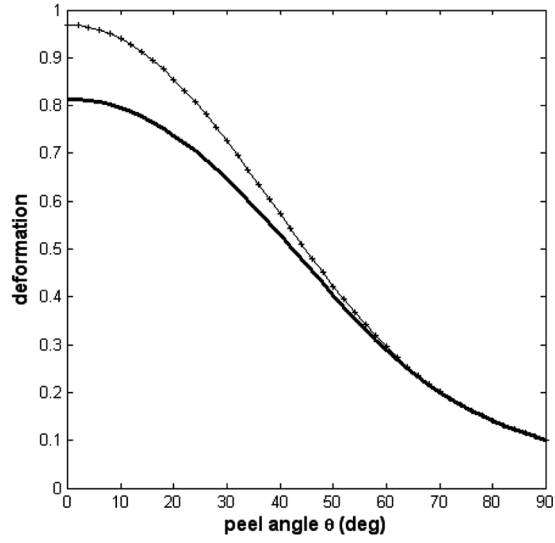

(b)

FIGURE 5 The conditions are the same as in Fig. 4 except for $B = 1.18\,\mathrm{N}$ which is smaller here (softer material). Note the difference between the results of the large deformation model Eq. (7), bold solid line, and those of Eq. (11) (model of Williams and Kauzlarich [6]), thin solid line with markers.

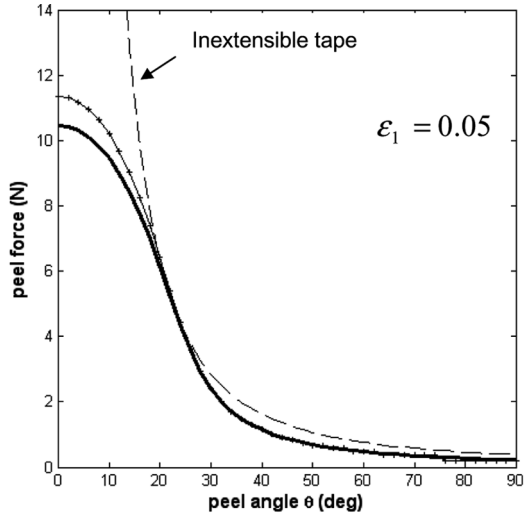

(a)

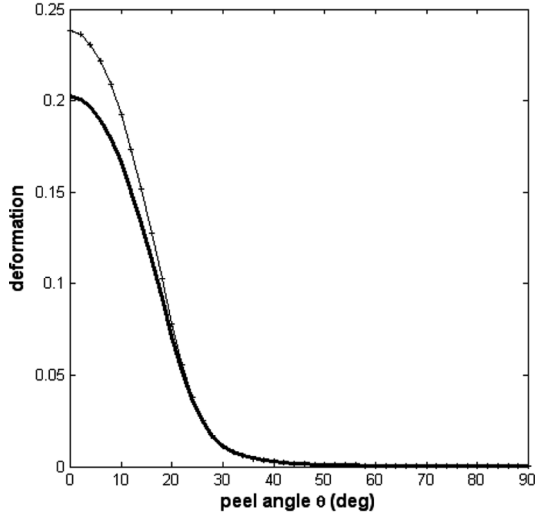

(b)

FIGURE 6 Effect of the pre-strain ($\varepsilon_1 = 0.05$) on (a) the peel force, (b) the tape deformation. The conditions are the same as those of Fig. 4 except for the pre-strain which was $\varepsilon_1 = 0$ in Fig. 4. To quantify the effect of pre-straining the results can be compared with those of Fig. 4. The predictions of Eq. (7) are the bold lines; those of Eq. (11) are the lines with markers. Note that the model accounting for tape extensibility merges with the inextensible solution at $\theta = 22^\circ$. Above this value the stored elastic energy helps the debonding and consequently the peeling force is smaller than for $\varepsilon_1 = 0$.

Fig. 6(a) shows that the peel force increases with ε_1 at small peel angles while it decreases at larger peel angles.

A critical value, ε_1^c, of the pre-strain can be defined, above which the stored elastic energy is large enough to produce a spontaneous debonding of the tape when no force is applied. This critical value is obtained by setting $F=0$ and $\varepsilon=0$ in Eq. (7). Thus, ε_1^c is the unique solution of the equation:

$$c(\varepsilon_1^c)=0, \tag{21}$$

where the function $c(.)$ is defined by:

$$c(\varepsilon_1)=\int_0^{\varepsilon_1} F(\varepsilon')\exp(\varepsilon')d\varepsilon' - \gamma b\exp(\varepsilon_1). \tag{22}$$

The uniqueness of the solution of Eq. (21) is demonstrated in Appendix C.

Note that the stored energy per unit length of the bonded tape is given by Eq. (3):

$$W_{el}^{BD}=\int_0^{\varepsilon_1} F(\varepsilon')\exp(\varepsilon'-\varepsilon_1)d\varepsilon'. \tag{23}$$

The condition in Eq. (21), defining the critical pre-strain for which spontaneous debonding occurs, is realized when the stored elastic energy becomes equal to the debonding energy per unit length, γb.

For the same conditions as those considered in Fig. 4 (tape characteristics given by a power law with $n=0.51$, $B=23.6\,\mathrm{N}$, decohesion energy $\gamma=20\,\mathrm{J/m^2}$), the critical pre-strain has the value $\varepsilon_1^c=0.08729$. Note that the assumption of small pre-strain is at its limit here. However, Eq. (7) is still used as a first approximation. The peeling force and the deformation in the detached tape are shown in Fig. 7 in terms of the peel angle in the case where the pre-strain is ε_1^c. Clearly, $\varepsilon=0$ is a solution of Eq. (7) due to Eq. (21) and the fact that $F=0$ for $\varepsilon=0$. Thus, at any peel angle, spontaneous debonding occurs for $\varepsilon=0$, *i.e.*, at a zero peel force. However, Fig. 7(b) shows also the existence of another root of Eq. (7) for $\theta<23.6^\circ$. In Appendix D, it is proved that for $\varepsilon_1<\varepsilon_1^c$ there is a unique solution of Eq. (7) for any value of the peel angle, θ, while for $\varepsilon_1\geq\varepsilon_1^c$ depending on the value of θ, there exists zero, one, or two solutions.

The solutions for deformations (ε) of Eq. (7) are shown in Fig. 7(b) by the bold solid lines. These lines define the limit between the domain where debonding is not feasible and the domain of dynamic debonding. At the limit between these domains a quasistatic and steady debonding is activated.

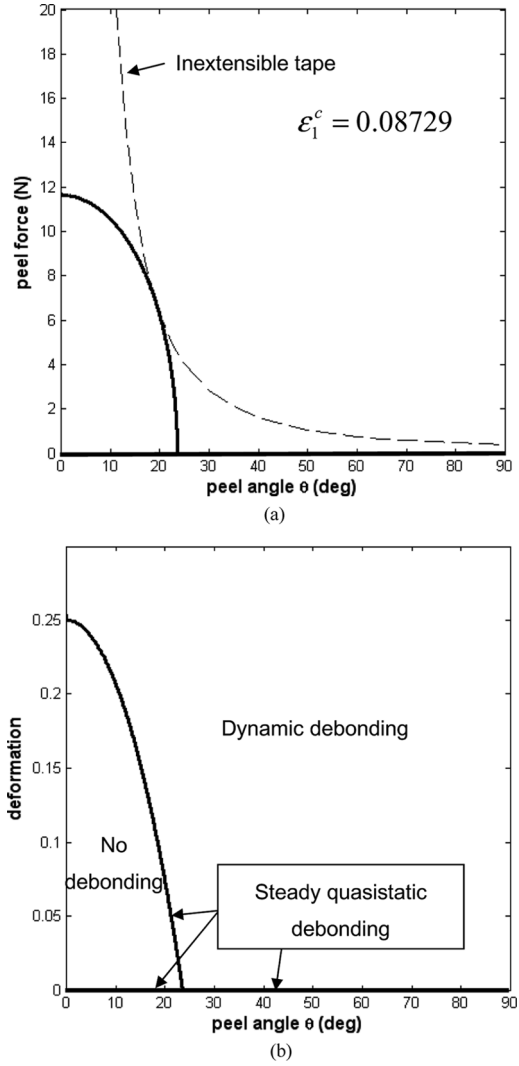

FIGURE 7 The tape has the same properties as in Figs. 4 and 6 but the prestrain is increased to the critical value $\varepsilon_1^c = 0.08729$ for which spontaneous debonding occurs for $F = 0$ at any peel angle θ. The bold solid lines in (a) and (b) correspond, respectively, to the values of the peeling force, F, and of the strain, ε, for which a steady quasistatic debonding is activated. These lines are the boundaries between domains where debonding is not possible and where dynamic debonding occurs. In (b), the bold solid lines represent the roots of Eq. (7). In addition to the root $\varepsilon = 0$, a second root exists for values of the peel angle smaller than $\theta_1 = \arccos(\exp(-\varepsilon_1^c))$, see Appendix D. Here, $\theta_1 = 23.6^\circ$.

In Fig. 8, the tape has same properties as in Figs. 4, 6, and 7 except for the pre-strain $\varepsilon_1 = 0.1$, which is larger than the critical value $\varepsilon_1^c = 0.08729$. The bold solid line in Figs. 8(a) and (b) correspond to states for which steady quasistatic debonding is activated. Note that

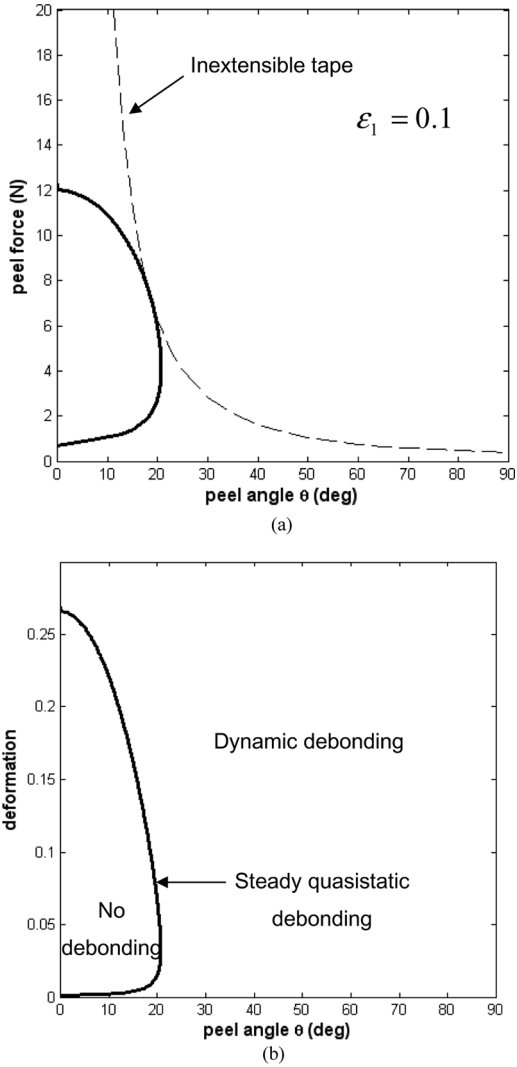

FIGURE 8 The tape has the same properties as in Figs. 4, 6, and 7 except for the pre-strain $\varepsilon_1 = 0.1$ which is larger than the critical value $\varepsilon_1^c = 0.08729$. The solid lines in (a) and (b) correspond to states for which steady quasistatic debonding is activated.

the solid line in (b) is easily obtained by observing that $\cos\theta$ is directly obtained in terms of ε from the relationship in Eq. (7). Then, the solid line in (a) is readily obtained in the parametric form $(\theta(\varepsilon), F(\varepsilon))$. For $\theta > 20.71^\circ$, Eq. (7) has no root for ε, while for $\theta < 20.71^\circ$, there are two positive roots; see the discussion in Appendix D.

It is worth discussing the results of Fig. 8 for the case $\theta = 0$. Figure 8(a) shows the existence of a segment [0.7 N, 12 N] of the peel force where no peeling occurs for any value of the force taken within this segment. Indeed, considering the case $F = 0$ for reference, the rate of external work is increased for any F taken inside the range [0.7 N, 12 N], but the increase is insufficient to compensate for the decrease of the elastic energy release rate. Indeed, the elastic energy remaining within the detached tape is increased for higher values of F; this is why the elastic energy release rate is reduced when F is increased.

Figure 9 shows, for different values of the pre-strain, the contour lines for which a steady quasistatic debonding does occur. This is an illustration of the results demonstrated in Appendix D concerning the uniqueness or the multiplicity of the roots of Eq. (7).

The results shown in Figs. 7–9 can be considered as "stability maps." These maps define the various domains in the peel-angle/peel-force plane. The first one is a domain of stable adhesion (no debonding is activated) and the second domain corresponds to dynamic debonding (catastrophic and uncontrolled process). The two domains are separated by a line where conditions of stable steady debonding are met. Figures 7–9 give a clear illustration of how the debonding process can be affected by the level of prestraining.

4. PROCESS ZONE MODEL

In general, the decohesion process takes place along a certain distance defining a process zone (or cohesive zone). Several process zone models have been developed in the literature for various tape responses; see, for example [4] and [10–15]. These models are aimed at defining the shape of the process zone and the energy dissipated during decohesion.

In this section, we consider the process zone model of Pesika *et al.* [4] accounting for the progressive decohesion of elastic tapes. The tape is still infinitely flexible [bending (flexion) work is neglected]. However, the tape has a finite curvature within the process zone. This curvature is related to the particular physics of the decohesion process, the flexible adhesive being drawn out into a series of fibrils. Pesika *et al.* [4] have considered the case of an inextensible tape. Here, the elastic deformation of the tape is included in the modelling and the effect of the pre-strain is also analysed.

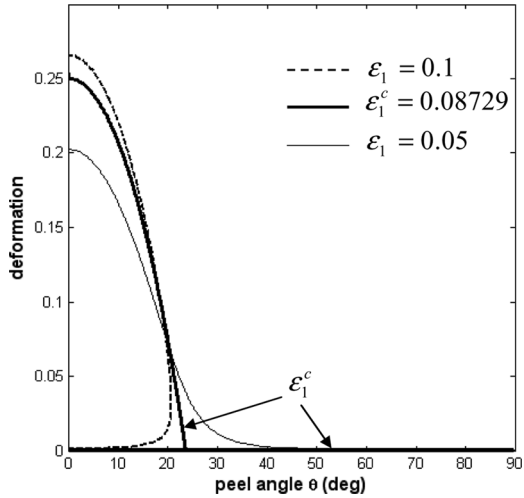

FIGURE 9 The tape has the same force-extension law (power-law with coefficients $n = 0.51$; $B = 23.6\,\mathrm{N}$) and same decohesion energy ($\gamma = 20\,\mathrm{J/m^2}$) as in Figs. 4, 6, 7, and 8. The roots of Eq. (7) are represented by different lines corresponding to the following values of the pre-strain $\varepsilon_1 = 0.05$ (subcritical), $\varepsilon_1^c = 0.08729$ (critical), and $\varepsilon_1 = 0.1$ (supercritical). For a given value of ε_1, the corresponding line represents the conditions for having a steady quasi-static decohesion process and is the limit between the domains of stable adhesion and dynamic debonding, see Figs. 7 and 8. As demonstrated in Appendix D, the Eq. (7) has a single root (thin solid line) in the subcritical case ($\varepsilon_1 < \varepsilon_1^c$), one or two roots (bold solid line) in the critical case ($\varepsilon_1 = \varepsilon_1^c$), and zero, one, or two roots (dashed line) in the supercritical case ($\varepsilon_1 > \varepsilon_1^c$).

4.1. The Peel-Zone Model of Pesika *et al.* [4] (PPZ Model) for Inextensible Tapes

The tape is first assumed to be inextensible. According to Pesika *et al.* [4], the decohesion process has two different regimes which are defined by the value of the peel angle, θ, with respect to a critical angle, ϕ_0 ($0 \le \phi_0 \le \pi/2$). Note that the tests conducted by these authors were limited to peel angles $0 \le \theta \le \pi/2$.

Regime I ($\phi_0 \le \theta \le \pi/2$)

The component $F_\perp$ of the peeling force orthogonal (perpendicular) to the substrate surface is independent of the peeling angle, θ. Thus, we have:

$$F = F_\perp / \sin\theta. \tag{24}$$

The incremental external work is still given by Eq. (6) where deformations are taken equal to zero (inextensible tape) and F is independent of deformation. Thus,

$$dW_{ext} = F(\theta)(1 - \cos\theta)dx. \tag{25}$$

The following material constant is introduced:

$$\gamma^* = F_\perp / b. \tag{26}$$

The incremental decohesion energy can be written as:

$$dW_{peel} = b\gamma dx. \tag{27}$$

The decohesion energy per unit surface, γ, is decomposed into reversible surface energy, γ_S (which is the sum of the contribution of the two surfaces created by debonding), and dissipated energy, $D(\theta)$:

$$\gamma = D(\theta) + \gamma_S. \tag{28}$$

In general, the dissipated energy depends upon the peel angle.

The energy balance for inextensible tapes has the form, $dW_{ext} = dW_{peel}$. By using Eqs. (24)–(28), we have:

$$D(\theta) + \gamma_S = \frac{\gamma^*(1 - \cos\theta)}{\sin\theta}. \tag{29}$$

Note that $D(\theta)$ is increasing with θ. Note also that the material constant γ^* is related to the energy dissipation at $\theta = \pi/2$ by $\gamma^* = D(\pi/2) + \gamma_S$.

Regime II ($0 \le \theta \le \phi_0$)

In the Regime II, the peel force depends on the peel angle as:

$$F(\theta) = b\gamma^* \left(\frac{\theta}{\phi_0}\right)\left(\frac{1 - \cos\phi_0}{1 - \cos\theta}\right)\frac{1}{\sin\theta}. \tag{30}$$

For $\theta = \phi_0$, the peeling force is $F(\phi_0) = b\gamma^* \frac{1}{\sin\phi_0}$, which matches with the value corresponding to Regime I given by (24) and (26). As for Regime I, considering that the tape is inextensible, the peeling energy per unit surface can be obtained from Eqs. (24)–(28):

$$D(\theta) + \gamma_S = \gamma^* \frac{1 - \cos\phi_0}{\phi_0}\frac{\theta}{\sin\theta}. \tag{31}$$

This expression matches with Eq. (29) for $\theta = \phi_0$.

4.2. Case of an Extensible Tape

Assume now that the tape can be elastically extended. It is assumed that peeling can be described by the process zone model [4]. The result in Eq. (7) can be used by replacing γ by

$$\frac{\gamma^*(1-\cos(\theta))}{\sin(\theta)} \quad \text{for} \quad \phi_0 \le \theta \le \pi/2:$$

$$F(\varepsilon)\exp(\varepsilon-\varepsilon_1) - F(\varepsilon)\cos(\theta) - \int_{\varepsilon_1}^{\varepsilon} F(\varepsilon')\exp(\varepsilon'-\varepsilon_1)d\varepsilon' - b\gamma^*\frac{1-\cos\theta}{\sin\theta} = 0, \tag{32}$$

and by replacing γ by $\gamma^*\frac{1-\cos\phi_0}{\phi_0}\frac{\theta}{\sin\theta}$ for $0 \le \theta \le \phi_0$:

$$F(\varepsilon)\exp(\varepsilon-\varepsilon_1) - F(\varepsilon)\cos(\theta) - \int_{\varepsilon_1}^{\varepsilon} F(\varepsilon')\exp(\varepsilon'-\varepsilon_1)d\varepsilon' - b\gamma^*\frac{1-\cos\phi_0}{\phi_0}\frac{\theta}{\sin\theta} = 0. \tag{33}$$

The model depends upon two parameters, γ^* and ϕ_0. The angle, ϕ_0, can be obtained from the measurement of the curvature of the backing and the length of the peel zone, see Pesika *et al.* [4]. The parameter γ^* is the adhesion energy at $\theta = 90^\circ$ and can be determined by a single test at $\theta = 90^\circ$ by assuming that the tape sustains negligible extension. The peeling force is then given by $F = b\gamma^*$. However, γ^* is frequently characterized by measurements at $\theta = \phi_0$. Note that γ^* is, in general, a function of the properties of the tape backing, of the adhesive, of the substrate, and of the detachment velocity. Note also that the peel-zone model of Pesika *et al.* [4] is retrieved when the tape extensibility is neglected ($\varepsilon = \varepsilon_1 = 0$).

4.3. Comparison of the Pesika *et al.*'s Peel-Zone Model [4] with Experimental Data

Pesika *et al.* [4] have used their model to characterize the peel test of adhesive tapes. Their experimental data are shown in Fig. 10 where the peel force per unit width (F/b) is represented in terms of the peel angle for a 3M 33 PVC electrical tape (squares) and for a composite tape (circles) made up of two layers, one of 3M 33 PVC electrical tape and one of 3M multitask Scotch^{TM} tape. The peel force is obtained by multiplying the results of Fig. 10 by the tape width, $b = 19\,\text{mm}$.

The dashed line represents the PPZ model. In this model, the tape is considered to be inextensible and the peel force, F/b, is given by Eq. (24) and (26) for $\phi_0 \leq \theta \leq \pi/2$ and by Eq. (30) for $0 \leq \theta \leq \phi_0$. For the electrical tape, the material parameters are $\phi_0 = 65^\circ$ and $\gamma^* = 270\,\mathrm{N/m}$.

A single layer of electrical tape has a relatively low stretching modulus which allows the tape to be significantly elongated during the peeling process. Therefore, the PPZ model which neglects the tape stretching cannot predict the peeling force for peel angles smaller than 50° (see Fig. 10a). By adding to the electrical tape a layer of 3M multitask Scotch tape, the composite tape so obtained has a higher stretching modulus while the adhesive properties remain identical to those of the electrical tape. The slight increase of the bending modulus of the composite tape is believed to have a negligible effect on the tape curvature which is assumed to be fully controlled by the adhesive strength. The peel-zone model is, therefore, the same for the composite tape and for the electrical tape. Since the stretching modulus of the composite tape is higher, the PPZ model is now able to predict correctly the experimental results for peel angles larger than 30° [dashed curve compared with circles in Fig. 10(a)]. However, for peel angles smaller than 30°, a divergence is still found between the peel-zone model and the experimental data.

The solid lines in Fig. 10(a) show the results of the peel-zone model accounting for the tape extensibility (elastic deformation). The model predictions are given by Eq. (32) for $\phi_0 \leq \theta \leq \pi/2$ and by Eq. (33) for $0 \leq \theta \leq \phi_0$. The values of ϕ_0 and of γ^* are the same as for the inextensible peel-zone model.

It is assumed that the pre-straining is equal to zero. For the 3M 33 PVC electrical tape (Layer #1) the force per unit width can be described, according to [6], by:

$$F_1 = a\frac{\varepsilon}{1+\varepsilon}, \tag{34}$$

with $a = 2{,}332\,\mathrm{N/m}$. The same tape was considered in Fig. 4. It can be noted that the power law used in Fig. 4, given also in [6], provides slightly different results at true strains smaller than 1 (no strains larger than 1 are reached in the cases studied here). Note also that the level of adhesion energy considered in Fig. 4 was much smaller than that of Fig. 10. For the second layer (3M multitask Scotch tape), the response is linear elastic:

$$F_2 = c\varepsilon, \tag{35}$$

with stiffness $c = 46{,}000\,\mathrm{Nm^{-1}}$ (tape thickness $40\,\mu\mathrm{m}$, the Young's modulus, E was measured as 1.15 GPa from tensile testing).

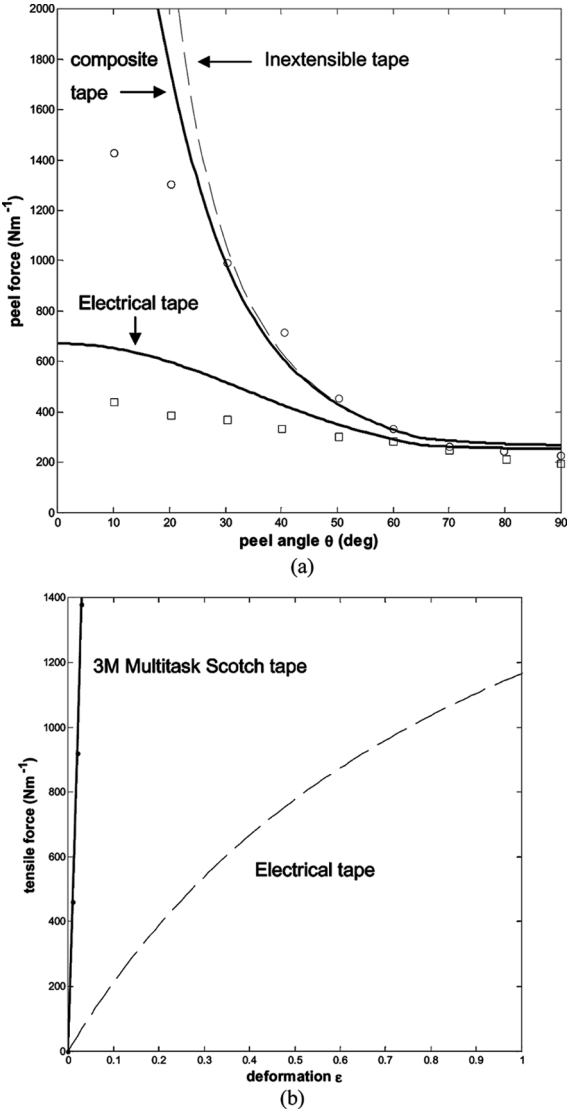

FIGURE 10 (a) Peel force per unit width (F/b) in terms of the peel angle θ. The experimental results of Pesika *et al.* [4] are represented by squares for the 3M 33 PVC electrical tape and by circles for the composite tape made up of two layers (Layer #1 is a 3M 33 PVC electrical tape, Layer #2 is a 3M multitask Scotch tape). The dashed curve is the peel-zone model of Pesika *et al.* [4] (PPZ model) for inextensible tape with parameters $\phi_0 = 65^\circ$ and $\gamma^* = 270\,\mathrm{N/m}$. The solid lines represent the results of the peel-zone model extended to account for the tape elastic deformation and for the constitutive models shown

Figure 10(b) shows the tensile response (force per unit tape-width in terms of deformation) for Layer #1 (dashed line) and Layer #2 (solid line). The response of the composite tape, obtained by addition of the tensile force of each individual layer, is close to those of Layer #2 and cannot be distinguished from the solid line in Fig. 10(b). This is due to the high stiffness of the 3M multitask Scotch tape which dominates the global response of the composite layer.

The solid lines in Fig. 10(a) represent the peel force per unit tape width for the Layer #1 (lower curve) and for the composite tape (upper curve). These results are obtained with the augmented peel-zone model (32), (33). The theoretical results for the 3M electrical tape show good agreement with the experiments of Pesika *et al.* [4] (square symbols) for peel angles larger than 60°. For lower values of the peel angle θ, a qualitative agreement is still found, but predictions of the model are stiffer than those of the experiments. For the composite tape, the agreement between the model, (32) and (33), and the experimental data is good for θ larger than 30° but is poor for small values of θ. Indeed, due to the high stiffness of the composite layer the predictions of the model, (32) and (33), are close to those of the inextensible model of Pesika *et al.* [4] [dashed line in Fig. 10(a)]. This raises the question about the factors contributing to the discrepancy between experimental data and model predictions at low peel angles.

The PPZ model [4] predicts that the decohesion energy is an increasing function of θ. The model assumes the existence of a stationary point at the exit of the peel zone. In this model, this point remains at the same distance from the substrate surface for all peel angles. This distance is determined by the value (assumed constant) of the tensile force of the last active filament. However, this hypothesis may not be valid when small peel angles are considered. In such cases, the adhesive layer sustains a shear dominant mode of deformation and the decohesion mechanism is likely to be different from the tensile mode of fibril elongation observed at large values of θ. It is expected

in Fig. 10(b) and described by Eq. (34) for Layer #1 and by Eq. (35) for Layer #2. The prestrain is $\varepsilon_1 = 0$. (b) Force per unit width as a function of the deformation ε for the Layer #1, 3M 33 PVC electrical tape (dashed curve) and the Layer #2, 3M multitask Scotch tape (solid line). The mechanical response of the composite layer (Layer #1 + Layer #2) is close to those of Layer #2 and cannot be distinguished on the graph. This is due to the high stiffness of the 3M multitask Scotch tape which dominates the response of the composite layer.

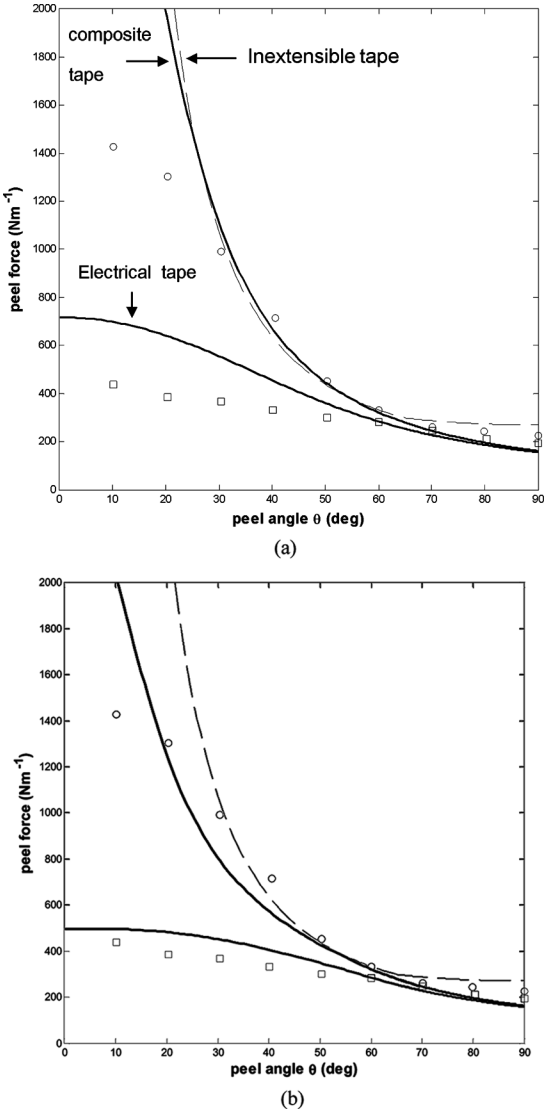

FIGURE 11 (a) Same configuration as in Fig. 10(a), except that the decohesion energy is assumed to be constant (independent of the peel angle). For the value $\gamma = 162\,\mathrm{N/m}$, the results shown by the solid curves (upper curve is for the composite tape, lower curve is for the electrical tape) are of the same quality as compared with those shown in Fig. 10(a) with the θ-dependent decohesion energy given by the PPZ model [4]. (b) The decohesion energy here has a maximum value of $\gamma_1 = 162\,\mathrm{N/m}$ at $\theta = 90^\circ$ and a minimum $\gamma_2 = 67.5\,\mathrm{N/m}$ at $\theta = 0^\circ$. The variation of the debonding energy with θ is given in the text. A

that, at small values of θ, the decohesion energy resulting from the shear mode of deformation will be smaller than those predicted by the PPZ model based on a fibril mode of decohesion. The decrease of the debonding energy associated with the shear mode should provide a better agreement with experimental data for small peel angles.

To evaluate the effect of the dependence of the decohesion energy upon θ, different decohesion models are compared in Fig. 11. In Fig. 11(a), we consider the most simple case where the decohesion energy γ is constant. Taking $\gamma = 162\,\mathrm{N/m}$ provides results of about the same quality, compared with the experimental data, than those in Fig. 10(a) where the debonding energy was given by the PPZ model [4]. For $\theta = 90^\circ$, the measured peel force is underestimated by the model with $\gamma = 162\,\mathrm{Nm}^{-1}$ and overestimated by the PPZ model (dashed line).

The decohesion model considered in Fig. 11(b) is defined by a maximum value of the decohesion energy γ_1 and a minimum value γ_2. It is assumed that the decohesion energy is constant for $\theta_1 \leq \theta \leq \frac{\pi}{2}$, where θ_1 is a given angle. The minimum value, γ_2, is assumed to be reached at $\theta = 0$. For $0 \leq \theta \leq \theta_1$, the variation of the decohesion energy in terms of θ is given by the polynomial expression $\gamma(\theta) = a_0 + a_1\theta + a_2\theta^2 + a_3\theta^3$, where the coefficients a_i are determined so as to satisfy the conditions $\gamma(\theta_1) = \gamma_1, \gamma(0) = \gamma_2, \frac{d\gamma}{d\theta}(\theta_1) = 0$, and $\frac{d\gamma}{d\theta}(0) = 0$. The results shown in Fig. 11(b) correspond to the following values of the model parameters: $\gamma_1 = 162\,\mathrm{N/m}$, $\gamma_2 = 67.5\,\mathrm{N/m}$, and $\theta_1 = 60^\circ$. These results provide a better agreement with the experimental data when compared with those using the PPZ model [4] [see Figs. 11(b) and 10(b)]. It seems difficult to have, with the same decohesion law, a good match of the experimental data for the electrical tape and the composite layer. This suggests that the decohesion energy might be affected by the addition of the 3M multitask Scotch tape to the electrical tape.

5. ADHESION OF A GECKO'S SPATULA

Pesika *et al.* [4] applied their peel zone model to analyse the adhesion of a gecko's spatula on a glass substrate. In this case, adhesion is due

better correlation is obtained with experimental results as compared with the models used in Figs. 10(a) and 11(a). However, it seems hard to have a good representation of the results for the electrical tape together with the composite layer. This suggests that the debonding energy may be affected by the addition of the multitask Scotch tape to the electrical tape.

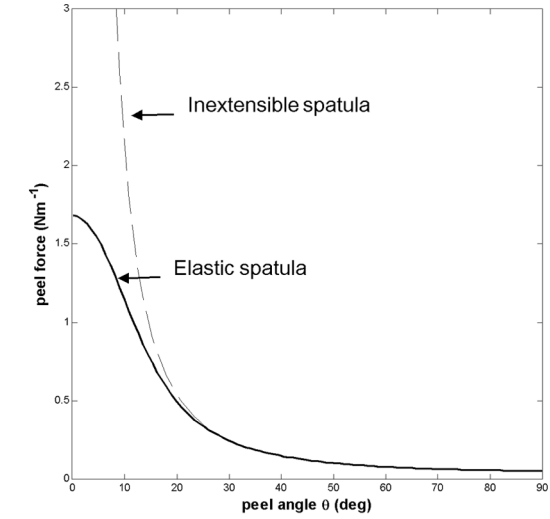

(a)

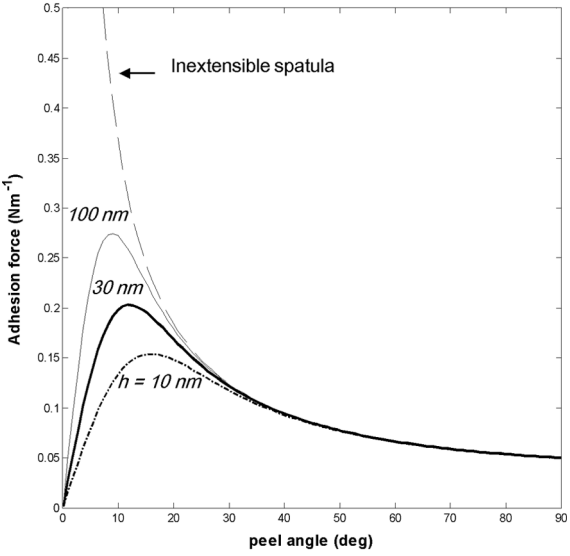

(b)

FIGURE 12 (a) Peel force per unit width in terms of the peel angle for a gecko's single spatula. The PPZ model (neglecting elastic effects) is represented by the dashed line. The model parameters are $\phi_0 = 90^\circ$ and $\gamma^* = 0.05\,\mathrm{N/m}$ for a glass substrate. The solid line shows the effects of elastic deformations of the gecko's spatula. (b) Adhesion force per unit width ($F_\perp/b$) of a spatula, for the PPZ model [4] (dashed line). Other curves show the effects of elastic deformations for a spatula with thickness $h = 10\,\mathrm{nm}$ (dotted curve),

to van der Waals forces. Thus, the concept of a cut-off distance to the substrate beyond which adhesive forces do not operate can be introduced. Due to the nature of van der Waals forces, this cut-off distance does not depend on the peel angle. Therefore, the PPZ model should work for the whole range of peel angles, while for adhesive tapes one observes limitations at small peel angles [see Fig. 10(a)].

The spatula pads are made up of β-keratin with Young's modulus of approximately 1.5 GPa [16]. In [4] the spatulae are considered to be sufficiently stiff to neglect extensibility. In Fig. 12(a) the peel force per unit width exerted on a single spatula is given in terms of the peel angle. The dashed line represents the PPZ model [4] with $\phi_0 = 90^\circ$ and $\gamma^* = 0.05\,\mathrm{N/m}$ for a glass substrate. Note that γ^*, the decohesion energy per unit surface for a peel angle of $\theta = 90^\circ$, was calibrated in [4] to be compatible with the measurement of the peel force by Huber *et al.* [17] for a single spatula. These authors measured the maximum pull force to be 10 nN for the peel angle $\theta = 90^\circ$. Indeed, as the width of the spatula is $b = 200\,\mathrm{nm}$, the maximum pulling force at $\theta = 90^\circ$ is $b\gamma^* = 10\,\mathrm{nN}$ (assuming negligible elastic deformation). The effect of the spatula's elastic extensibility is illustrated in Fig. 12(a) (bold solid line). The thickness of the spatula is taken as $h = 30\,\mathrm{nm}$. Results are obtained using Eq. (33) and are similar to those of Kendall's model. It is observed that elastic effects become substantial for a peel angle lower than 20°.

In Fig. 12(b), we report the adhesion force per unit width, $F_\perp/b = F/b\sin(\theta)$, in terms of the peel angle. The same data and equations are used as for Fig. 12(a). The dashed line refers again to the PPZ model [4] for inextensible spatula. When elastic effects are accounted for, the adhesion force shows a maximum load bearing capacity which depends on the spatula's stiffness. For $h = 30\,\mathrm{nm}$, the maximum of the adhesion force is given in Fig. 12(b) by $F_\perp^{spatula}/b = 0.203\,\mathrm{N/m}$ for the value of the peel angle $\theta = 11.8^\circ$. Thus, for a single spatula with width $b = 200\,\mathrm{nm}$, the maximum of the adhesion force is $F_\perp^{spatula} = 40.6\,\mathrm{nN}$. Considering that a seta contains about 1000 spatulae, it is worth noting that for a single seta the maximum of the predicted adhesion force by the present model is $F_\perp^{seta} = 40.6\,\mu\mathrm{N}$. This value is very close to the

30 nm (bold solid line), and 100 nm (thin solid line). The adhesion force has a maximum load bearing capacity when elastic effects are taken into account. Note that for $h = 30\,\mathrm{nm}$, the maximum of the adhesion force is $0.203\,\mathrm{N/m}$. This value provides a maximum adhesion force for a single seta in agreement with experimental measurements.

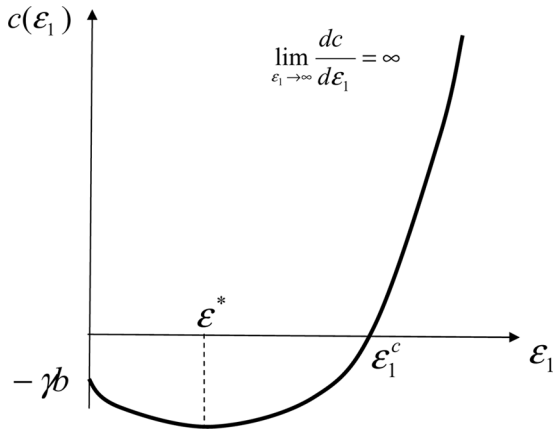

FIGURE 13 Schematic representation of the function $c(\varepsilon_1)$ defined by the Eq. (22).

measured adhesion force reported in the literature, [2] and [4]. These results depend on the tensile stiffness of the spatula which, for a given width b, is proportional to the thickness h. In the literature, h is reported to decrease along the spatula length with a minimum value of 10 nm at the tip of the spatula. However, there is a certain scatter in the evaluation of the maximum value of h (at the base of the spatula) between 30 and 100 nm. For comparison, we have reported in Fig. 12(b) the effects of the spatula's thickness on the adhesion force for $h = 10$, 30 and 100 nm.

6. CONCLUSIONS

The peeling test of non-linear elastic tapes has been described by developing a general framework accounting for large deformations, tape pre-straining, and the gradual debonding of the tape along a process zone. The introduction of a large deformation setting is a new aspect of the modelling, which is motivated by potential applications to soft polymers and tissues, especially in bioengineering. Non-linear material response and large extensibility are important features which are fully accounted for by the present model.

A parametric analysis has been developed to show how large deformations of the tape could affect the peeling force. The pre-strain introduced into the tape during the bonding operation can also have important implications on the debonding process. "Stability maps" have been obtained in the peel-angle/peel-force plane for the case of

force control. In the stability map two domains can be distinguished, the first being a domain of stable adhesion (where no debonding is activated) and the second being a domain of dynamic debonding (catastrophic and uncontrolled process). The two domains are separated by a line where conditions of steady debonding are met.

The decohesion energy associated with a given process-zone model can be easily included in the formulation of the peeling model. The process-zone is the region where the tape is progressively detached from the substrate. As an example, the process-zone model of Pesika *et al.* [4] (PPZ) initially developed for inextensible adhesive tapes has been extended here by accounting for elastic deformations. The results of the model have been compared with the experimental data of Pesika *et al.* [4] for adhesive tapes. They are found to be in good quantitative agreement with experimental data for large values of the peel angle and in qualitative agreement for small peel angles. It is noted that, for adhesive tapes, the value of the decohesion energy predicted by the PPZ model [4] might be too large at small peel angles. However, when the gecko's adhesion is considered, adhesion is due to Van der Waals forces and the PPZ model can be viewed as valid in the whole range of peel angles.

We have evaluated the maximum adhesion force of a single gecko's spatula by combining the PPZ model and elastic effects. The theoretical prediction was found to be well correlated to the measurement of the maximum load bearing capacity of a gecko's seta reported in the literature.

ACKNOWLEDGMENTS

GR gratefully acknowledges the support provided by the National Science Foundation (DMR #0520565) through the Center for Science and Engineering of Materials (CSEM) at the California Institute of Technology. We thank Christopher Kovalchick for obtaining the mechanical characteristics of the 3M multitask Scotch tape.

REFERENCES

[1] Autumn, K., Liang, Y. A., Hsien, S. T., Zesch, W., Chan, W. P., Kenny, T. W., Fearing, R., and Full, R., *Nature* **405**, 681–685 (2000).
[2] Autumn, K., Sitti, M., Liang, Y. A., Peattie, A. M., Hansen, W. R., Sponberg, S., Kenny, T. W., Fearing, R., Israelachvili, J. N., and Full, R. J., *PNAS* **99**, 12252–12256 (2002).
[3] Yao, H. and Gao, H., *J. Mechanics Physics Solids* **54**, 1120–1146 (2006).
[4] Pesika, N. S., Tian, Y., Zhao, B., Rosenberg, K., Zeng, H., McGuiggan, P., Autumn, K., and Israelachvili, J. N., *J. Adhes.* **83**, 383–401 (2007).
[5] Tian, Y., Pesika, N. S., Zeng, H., Rosenberg, K., Zhao, B., McGuiggan, P., Autumn, K., and Israelachvili, J., *PNAS* **103**, 19320–19325 (2006).

[6] Williams, J. A. and Kauzlarich, J. J., *Tribology International* **38**, 951–958 (2005).
[7] Rivlin, R. S., *Paint Technol* **9**, 215–216 (1944).
[8] Kendall, K., *J. Phys. D Appl. Phys.* **8**, 1449–1452 (1975).
[9] Williams, J. A. and Kauzlarich, J. J., *J. Adhes.* **80**, 433–458 (2004).
[10] Kaelble, D. H., *Trans. Soc. Rheol.* **3**, 161–180 (1959).
[11] Kaelble, D. H., *J. Adhes.* **1**, 102–123 (1969).
[12] Chen, W. T. and Flavin, T. F., *IBM J. Res. Devel.* **23**, 203–213 (1972).
[13] Kim, K.-S. and Aravas, N., *Int. J. Solids Struct.* **24**, 417–435 (1988).
[14] Wei, Y. and Hutchinson, J. W., *Int. J. Fract.* **93**, 315–333 (1988).
[15] Georgiou, I., Hadavinia, H., Ivankovic, A., Kinloch, A. J., Tropsa, V., and Williams J. G., *J. Adhes.* **79**, 239–265 (2003).
[16] Autumn, K., Majidi, C., Groff, R. E., Dittmore, A., and Fearing, R., *J. Experimental Biology* **2009**, 3558–3568 (2006).
[17] Huber, G., Gorb, S. N., Spolenak, R., and Arzt, E., *Biol. Lett.* **1**, 2–4 (2005).

APPENDIX A: ELASTIC ENERGY

Consider a tape element with length L_0 in the stretch free state (no deformation). During the bonding process with the substrate, this element is stretched to a length L and the strain after bonding is $\varepsilon_1 = \ln(L/L_0)$, which is the pre-strain. When the element is completely detached from the substrate the length has the value l and the strain is $\varepsilon = \ln(l/L_0)$. During stretching from L_0 to L the elastic energy is identical to the work of the tensile force F. Thus, the elastic energy stored in the tape element before debonding (BD) is:

$$\begin{aligned} W_{el}^{BD} &= \int_{L_0}^{L} F(L')dL' = L_0 \int_0^{\varepsilon_1} F(\varepsilon') \exp(\varepsilon')d\varepsilon' \\ &= L \int_0^{\varepsilon_1} F(\varepsilon') \exp(\varepsilon' - \varepsilon_1)d\varepsilon'. \end{aligned} \tag{A1}$$

Similarly, after complete detachment (AD) the elastic energy has the form:

$$W_{el}^{AD} = L_0 \int_0^{\varepsilon} F(\varepsilon') \exp(\varepsilon')d\varepsilon' = L \int_0^{\varepsilon} F(\varepsilon') \exp(\varepsilon' - \varepsilon_1)d\varepsilon'. \tag{A2}$$

APPENDIX B: DEPENDENCE OF THE BONDING ENERGY (PER UNIT AREA), γ_1, OF ATTACHED TAPE UPON THE BONDING ENERGY (PER UNIT AREA), γ, OF THE UNSTRETCHED TAPE

The bonding energy (per unit area), γ_1, of attached tape should at least depend upon the pre-strain, ε_1, and the bonding energy (per unit area), γ, of the unstretched tape. The general formulation of this functional

dependence is hardly accessible, and should be a function of the physical and chemical properties of the surfaces considered. We develop here the analysis under the simple assumption that the bonding energy of the stretched element, $\gamma_1 b_1 dx$, is identical to the bonding energy of the unstretched element with area, $b\,dL_0$:

$$\gamma_1 b_1 dx = \gamma b\, dL_0. \tag{B1}$$

Considering that $dL_0 = \exp(-\varepsilon_1)dx$, it follows that:

$$\gamma_1 b_1 = \gamma b \exp(-\varepsilon_1). \tag{B2}$$

Thus, Eq. (6) can be written as:

$$F(\varepsilon)\exp(\varepsilon - \varepsilon_1) - F(\varepsilon)\cos(\theta) - \int_{\varepsilon_1}^{\varepsilon} F(\varepsilon')\exp(\varepsilon' - \varepsilon_1)d\varepsilon' - \gamma b \exp(-\varepsilon_1) = 0. \tag{B3}$$

It is worth noting that, for a small pre-strain, ε_1, the relationship Eq. (7) is retrieved.

It is also interesting to mention that (B1) can be elegantly expressed, in terms of the stretches $\lambda = \frac{dl}{dL_0} = \exp(\varepsilon)$ and $\lambda_1 = \frac{dx}{dL_0} = \frac{dL}{dL_0}$, as:

$$(\lambda - \lambda_1 \cos\theta)F(\lambda) - \int_{\lambda_1}^{\lambda} F(\lambda')d\lambda' - \gamma b = 0. \tag{B4}$$

APPENDIX C: UNIQUENESS OF THE ROOT, ε_1^c, OF THE EQUATION $c(\varepsilon_1^c) = 0$

From the definition Eq. (22) of the function $c(\varepsilon_1)$ we have:

$$\frac{dc}{d\varepsilon_1} = (F(\varepsilon_1) - \gamma b)\exp(\varepsilon_1). \tag{C1}$$

Since $F(\varepsilon_1) = B\varepsilon_1^n$ is strictly increasing, and since $F(0) = 0$, there exists a number $\varepsilon^* > 0$ such that,

$$\frac{dc}{d\varepsilon_1} < 0 \quad \text{for } 0 \le \varepsilon_1 < \varepsilon^*,$$

$$\frac{dc}{d\varepsilon_1} = 0 \quad \text{for } \varepsilon_1 = \varepsilon^*,$$

$$\frac{dc}{d\varepsilon_1} > 0 \quad \text{for } \varepsilon^* < \varepsilon_1.$$

Since $c(0) = -\gamma b < 0$ and $\lim_{\varepsilon_1 \to \infty} \frac{dc}{d\varepsilon_1} = \infty$, there is a single root, ε_1^c, of the equation $c(\varepsilon_1^c) = 0$, as illustrated in Fig. 13.

The following results are also used in the paper:

$$\begin{aligned} c(\varepsilon_1) &< 0 \quad \text{for } \varepsilon_1 < \varepsilon_1^c, \\ c(\varepsilon_1) &= 0 \quad \text{for } \varepsilon_1 = \varepsilon_1^c, \\ c(\varepsilon_1) &> 0 \quad \text{for } \varepsilon_1 > \varepsilon_1^c. \end{aligned} \tag{C2}$$

APPENDIX D: ROOTS OF EQUATION (7)

For given values of the pre-strain, ε_1, and of the peel angles, θ, let us define the function $H(\varepsilon)$ as:

$$H(\varepsilon) = G(\varepsilon, \varepsilon_1, \theta) - G_c, \tag{D1}$$

where G is the energy release rate defined by Eq. (14) and $G_c = \gamma$ is the decohesion energy per unit area.

Note that the roots, ε, of the equation

$$H(\varepsilon) = 0, \tag{D2}$$

are identical to those of Eq. (7). From the definition Eq. (22) of $c(.)$ and considering that $F(0) = 0$, we have:

$$H(0) = \frac{1}{b} \exp(-\varepsilon_1) c(\varepsilon_1).$$

It follows from (C2) that:

$$\begin{aligned} H(0) &< 0 \quad \text{for} \quad \varepsilon_1 < \varepsilon_1^c, \\ H(0) &= 0 \quad \text{for} \quad \varepsilon_1 = \varepsilon_1^c, \\ H(0) &> 0 \quad \text{for} \quad \varepsilon_1 > \varepsilon_1^c. \end{aligned} \tag{D3}$$

Considering the derivative of (D1) with respect to ε, it follows that:

$$\frac{dH}{d\varepsilon} = \frac{1}{b} \frac{dF}{d\varepsilon} (\exp(\varepsilon - \varepsilon_1) - \cos\theta). \tag{D4}$$

It is assumed that $\frac{dF}{d\varepsilon} > 0$ for $\varepsilon \geq 0$ and that $\lim_{\varepsilon \to \infty} \exp(\varepsilon) \frac{dF}{d\varepsilon} = +\infty$. Note that these conditions are in particular fulfilled for the power law Eq. (20). Note also that, from (D4), we have:

$$\lim_{\varepsilon \to \infty} \frac{dH}{d\varepsilon} = +\infty. \tag{D5}$$

Clearly, there exists a unique ε^* (possibly negative) such that the quantity $(\exp(\varepsilon - \varepsilon_1) - \cos\theta)$ is strictly negative for $\varepsilon < \varepsilon^*$, zero for $\varepsilon = \varepsilon^*$, and strictly positive for $\varepsilon^* < \varepsilon$. Thus, from (D4) the function

$$\varepsilon \to H(\varepsilon) \text{ is strictly decreasing for } \varepsilon < \varepsilon^* \text{ and strictly increasing for } \varepsilon^* < \varepsilon. \tag{D6}$$

The discussion of the roots of Eq. (7) depends on the value of the prestrain ε_1.

Case, $\varepsilon_1 < \varepsilon_1^c$

According to (D3) we have $H(0) < 0$. Considering, in addition, the results (D5) and (D6) it appears that there exists a unique root $\varepsilon > 0$ of (D2).

Case, $\varepsilon_1 = \varepsilon_1^c$

From (D3), we have $H(0) = 0$. Thus, $\varepsilon = 0$ is a root of Eq. (D2) and (7). However, depending on the value of the peel angle another root may exist. Let us define θ_1 by $\theta_1 = \arccos(\exp(-\varepsilon_1^c))$. Note that $0 \le \theta_1 \le \pi/2$. From (D4), we have

$$\frac{dH}{d\varepsilon}(0) = \frac{1}{b}\frac{dF}{d\varepsilon}(0)(\cos\theta_1 - \cos\theta). \tag{D7}$$

Thus, the number of roots of (D2) depends on θ.

For $\theta_1 < \theta \le \pi/2$ we have $\frac{dH}{d\varepsilon}(0) > 0$. Considering that $H(0) = 0$ and (D6), there is no root different from $\varepsilon = 0$.

For $\theta = \theta_1$, $\frac{dH}{d\varepsilon}(0) = 0$. Thus, $\varepsilon^* = 0$ and $\frac{dH}{d\varepsilon}(\varepsilon) > 0$ for $\varepsilon > 0$. There is again a single root, $\varepsilon = 0$.

For $0 \le \theta < \theta_1$, $\frac{dH}{d\varepsilon}(0) < 0$. Thus, according to (D6), $\varepsilon^* > 0$ and there exists a second root $\varepsilon > 0$ of Eq. (D2) or (7).

These results are in agreement with those of Fig. 7(b).

Case, $\varepsilon_1^c < \varepsilon_1$

From Eq. (D3), $H(0) > 0$. Introducing the angle $\theta_1 = \arccos(\exp(-\varepsilon_1))$, $0 \le \theta_1 \le \pi/2$, the relationship Eq. (D7) is still valid. Thus, for $\theta_1 \le \theta \le \pi/2$, we have $\frac{dH}{d\varepsilon}(0) \ge 0$ and, since $H(0) > 0$, there is no root for Eq. (D2) or (7). For $0 \le \theta < \theta_1$, we have $\frac{dH}{d\varepsilon}(0) < 0$ and therefore, according to (D6), the deformation ε^*, for which $H(\varepsilon)$ is minimum, is strictly positive. Since $H(0) > 0$, three situations can be found [as shown in the Fig. 8(b)] depending on the value of θ: there exists zero, one, or two roots.